Microsystem Technologies (2019) 25:4019–4025
https://doi.org/10.1007/s00542-019-04406-2

TECHNICAL PAPER

3D-printed membrane microvalves and microdecoder

Zhou Zhou[1] · Gonghan He[1] · Kunpeng Zhang[1] · Yang Zhao[1] · Daoheng Sun[1]

Received: 30 November 2018 / Accepted: 18 March 2019 / Published online: 10 April 2019

Abstract
A microfluidic system for multichannel switching and multiphase flow control has potential uses in pneumatic soft robotics and biological sampling systems. At present, the membrane microvalves used in microfluidic systems are mostly constructed using a multilayer bonding process so that the device cannot withstand high pressures. In this paper, we demonstrate a design method and the properties of a bondless membrane microvalve fabricated using a commercial 3D printer. We used a multijet (MJP) 3D printer to print a 100-μm-thick and 6-mm-diameter membrane from a relatively hard material (1700 MPa). The membrane's high toughness ensures that it does not need negative pressure to reopen. The measured operation frequency was less than 2.5 Hz under a pneumatic pressure of 14.5 kPa. We also 3D-printed an integrated Quake-style microfluidic decoder network by combining 8 valves in series to demonstrate the integrability of the microvalve. The decoder chip was demonstrated to control the ON/OFF state of the four coded fluidic channels, with the droplets being generated from selected channels according to the valve action. Therefore, such 3D-printed microvalves are highly integrable, have a high manufacturing efficiency, and can be applied in pneumatic controllers, sample switchers and integrated print heads.

1 Introduction

At present, microfluidic technology is developing rapidly, with applications extending from traditional bioinstrumentation to automatic pneumatic processors. The original bonded chips generally do not need to consider high-pressure situations when actuated by a low-pressure syringe pump. However, they face structural reliability problems caused by a high operating pressure when used as a microfluidic pneumatic processor. The pressure on the controller in this application is usually 100 kPa or higher, which puts forward more stringent requirements for the mechanical structure and robustness.

The Quake group first introduced normally open valves with a very simple three-layer sandwich structure made from PDMS (Fig. 1a) (Unger et al. 2000). Due to the functional similarity between microfluidics and electrical circuits, they defined it as a fluidic diode. Subsequently, systems consisting of such units became known as digital microfluidics (Lederer et al. 2012; Jain et al. 2015; Scott-Murrell et al. 2017), microfluidic automation (Kim et al. 2012; Au et al. 2015) or microfluidic circuitry (Frank et al. 2017). The integration method is a challenge in the processing of micro/nanodevices for IC or microfluidic chips (Cho et al. 2002; Oh et al. 2012); however, few studies have been reported on this topic. A large-scale microfluidic logic network was presented (Thorsen et al. 2002) and successfully implemented in a microfluidic system according to the fluid properties. Based on this idea, many bio/chemical switching chips based on microfluidic technology have been developed (Gong et al. 2016; Ma et al. 2009; Jensen et al. 2010; Kawai et al. 2015). The current PDMS chip can control multichannel fluids. However, this original lithography-bonding processed structure still operates at relatively low pressures (Lu et al. 2007). The pressure that it can withstand is limited by the PDMS bonding force, which is approximately 100 kPa for reversible bonding.

As an excellent approach of once-molded production for integrated devices, 3D printing technology is entering a new period because new deposition methods based on optical technologies are available and are replacing the traditional hot squeeze methods, such as stereo lithography (SLA), digital light processing (DLP) and multijet modeling (Bhattacharjee et al. 2016). Many support materials can be easily removed by organic solvents without surface damage using these new methods (Zhu et al. 2014, 2015).

✉ Daoheng Sun
sundh@xmu.edu.cn

[1] Department of Mechanical and Electrical Engineering, Xiamen University, South Xiang'an Road, Xiamen, China

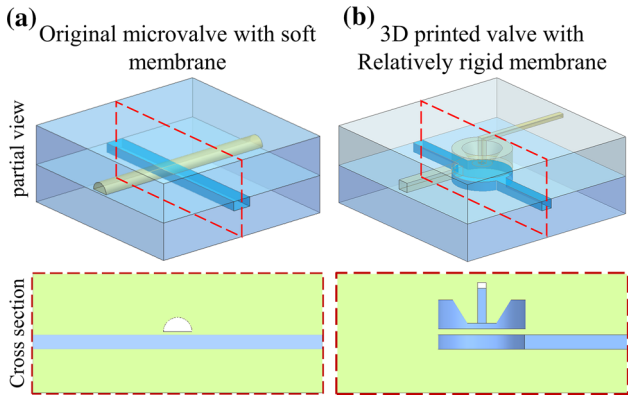

Fig. 1 Isometric and cross-section views of the valves. **a** Original membrane valve design, with a staggered flow path. **b** Our 3D-printed membrane valve design, with a boss in the upper sample flow cavity

3D printing technologies represent a new fabrication approach in the micropneumatic control field (Rhee and Burns 2009; Brockmeyer et al. 2015). Although they have been studied for years, most of these 3D printed components are still used as passive chemical reaction containers without movable structures (Kazenwadel et al. 2016; Kadimisetty et al. 2018). The introduction of 3D-printed movable structures into microfluidic systems could enable many more functions, ranging from drivers to control systems (Sochol et al. 2015). The feasibility of such structures has been proven in industrial applications (Rogers et al. 2015; Hua et al. 2016; Gong et al. 2018). Several reports also demonstrated that the biocompatibility of 3D print materials has enabled feasible advances in the study of cytology and drug discovery (Jia et al. 2016; Knowlton et al. 2016; Sweet et al. 2017; Munshi et al. 2018). For such demands, more suitable 3D printing methods have been used to provide large-scale microfluidic fabrication, and different printing methods will result in different structural compositions and material performances. A 3D-printed microfluidic chip was produced at the submillimeter scale based on the SLS method and integrated with intricate components, such as a membrane-like valve, within the microchannels to regulate fluid flow (Moore et al. 2011; Gong et al. 2016; Lee et al. 2016). A device should contain a set of valves, and the functions could correspond to electronic components used in logic operations. Series and parallel connections were applied to connect several valves together using the SL method, and automated feeding and switching at the several-millimeter scale was realized (Wehner et al. 2016; Lee et al. 2018). In these devices, the key structure is a membrane consisting of a single layer. Both its static (e.g., size or strength) and dynamic (e.g., deformable or movable) characteristics have a considerable influence on the physical properties, such as the response time and service life (Garcia-Cordero et al. 2010). Performance defects can be caused by support material residue or structural abrasion during the post-treatment process. Based on a surface-friendly solvent-removal method, multijet printing (MJP) technology was used to examine a fundamental class of 3D-printed microfluidic operators, including fluidic capacitors, fluidic diodes, and fluidic transistors (Sochol et al. 2015).

Currently, 3D print microvalves and micropumps are always used in passive flow control without movable structures (Zhu et al. 2014). Here, we present a modified version of the original membrane valve (Fig. 1b) that can be 3D-printed from acrylic plastics. An integrated microfluidic decoder network is demonstrated to verify the feasibility of the fabrication of an integrated microvalve array by a one-step 3D print process. The properties of this 2^n decoding chip were investigated.

2 Design and fabrication

A mechanical solvent-removal approach called MJP was chosen to realize the integration and multilayer structure of this chip (Zhu et al. 2015). This method consist of three parts: print head, UV lamp and a precision high-speed roller. When print head prints layers of UV curable liquid plastic onto a flat platform, wax support (Visijet S300, 3D systems) material also jetted to void and other freedom surface. A high speed roller is used to make a smooth upper surface for the next layer. After 5–6 s UV exposure, a fully cured plastic layer was created. Using this method, the support material in an untreated chip can undergo hands-free, melt-away removal from even the most inaccessible geometry features while avoiding surface damage. A hydroxylated wax that can dissolve in oil or react with a polar organic solvent without dissolving the structural material was essential in this research.

VisiJet M3 Crystal (3D Systems, SC; $\rho = 1.02 \times 103$ kg/m^3; E = 1460 MPa), were used to perform all of the research. In previous reports, VisiJet Crystal is a USP Class VI Certified material and has been assessed for use in zebrafish embryo test (Macdonald et al. 2016). The material maintains excellent chemical stability for low-concentration non-toxic or low-toxic solvents, and is soluble only in solvents such as chloroform and dichloromethane which are not commonly used in biological experiments.

The material has similar optical properties (nd = 1.57, Vd = 59) to the general photosensitive resin, but since the surface of the 3D printing exhibits a stripe-like unevenness distribution, There is a strong diffuse reflection on the surface, which affects the optical properties of the structure (Fig. 2a, b). In practice, it is not suitable as an observation structure for chemical reactions, cells or even an image

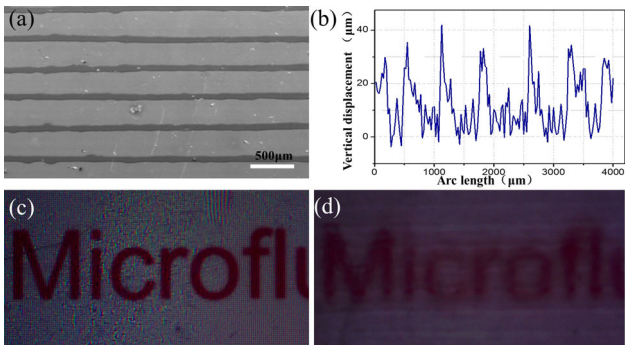

Fig. 2 3D printing surface topography and optical properties. **a** Surface topography under optical microscope. **b** Surface roughness test. **c** Imaging characteristics by pouring method. **d** Imaging characteristics by MJP method

(Fig. 2c, d). For non-optical observation structures, the material can maintain the uniform shape of the flow channel due to its high strength characteristics and 3D structure character which is very suitable for the mixing, separation and flow adjustment modules of the front end processing of the microfluidic system.

The architecture and functional principle of the valve are shown in Fig. 3. When zero pressure is applied to the control channel, the membrane stays the same and the upper flow channel remains open; when pressure is applied, the membrane deflects and closes the flow channel. The 3D printed-membrane is a typical clamp-supported structure, and the stress concentration is particularly high on the edge, leading to breakage and even causing partial cracks. To reduce the membrane strain required to close the valve,

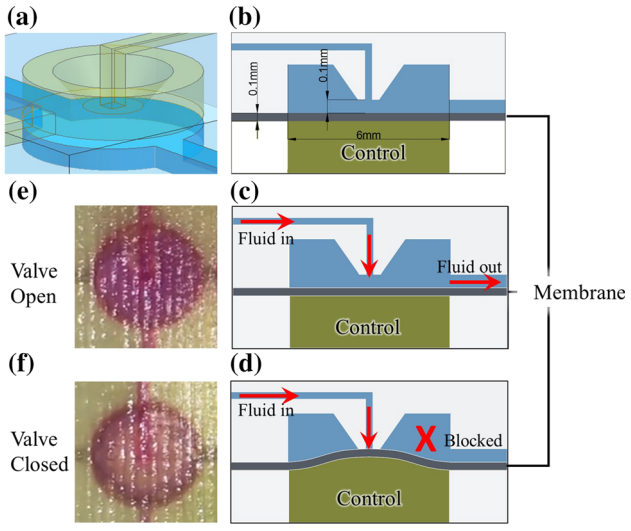

Fig. 3 Design and operation principle of the microvalve. **a** Isometric view of a functional microvalve. **b** Cross-sectional view of the valve. **c**, **d** The open/closed mode is controlled by a movable membrane in the cavity. **e** Micrograph of the valve in its open state, with no pressure applied to the control channel. **f** Micrograph of the valve in its closed state (20 kPa applied)

we designed a lug boss in the sample flow cavity and fabricated a vertical inlet channel (Fig. 3a, b), so that the membrane (diam: 6 mm, thickness: 100 μm) could easily reach the valve seat and seal the valve (Fig. 3d, f).

The deformation of a clamp-supported circuit membrane could be described as Cheng (2008):

$$P_c r^4 / E t^4 = 5.33 w_0 / (1 - v^2) t + 2.6 w_0^3 / (1 - v^2) t^3, \quad (1)$$

where Pc is the uniformly distributed load on the membrane, ω_0 is the membrane's normal deflection in the closed stage, ranging up to 100 μm (3 layers) in this printing process to guarantee the complete release of the structure, and t is the membrane thickness, which was set to 100 μm to provide sufficient sealing and robustness. ν is the Poisson's ratio of the material, measured as 0.35. The Young's modulus E of this material is 1463 MPa. According to Eq. 1, there is a nonlinear relationship between the membrane radius and pressure. For a target vertical deflection of 100 μm, the rate of decrease in the required pressure was rapidly approached when the radius exceeded 6 mm, which was considered the optimal size for our construction.

Casting wax can be easily removed from the external surfaces of the device by immersion in vegetable oil at 65 °C. However, the high-viscosity oil cannot easily flow into the inner channels because of the surface tension. The removal process becomes more difficult with reductions in the cross-sectional area and increases in the channel length. For the cost efficiency experiment, all channels were fabricated with a cross-sectional size of 600 × 400 μm (width × height). A cut-through channel was designed in our chip instead of a dead volume channel (Fig. 4a, b). A circulating pump system was connected to each entrance to remove the support wax completely. The chip was immersed in the oil groove, which was heated to 65 °C, and the flow rate of the pump was maintained at 5 mL/min to ensure an appropriate scouring force to clear off the inner surfaces, particularly the membrane. After the oil treatment, the heater was turned off, and the oil was replaced with isopropanol. The alcohol was injected cyclically to remove the remaining wax and oil, particularly the dead volume. Compared with the simple immersion method, the injection method can completely remove the wax in 1 h (Fig. 4c). According to the microscope image (Fig. 4d), the treated structure has a dentation height of approximately 20 μm along the height direction. Such features are common in the layer-by-layer printing method and cannot be removed from the inner wall. Because the manufacturing surface roughness is less than Ra 3.2, its effect on the flow resistance can be disregarded in experiments on low-Re flow (< 200) according to the Churchill formula (Cheng 2008). After treatment, the exit end of the control channel was sealed off by resin material to guarantee the control of the pressure.

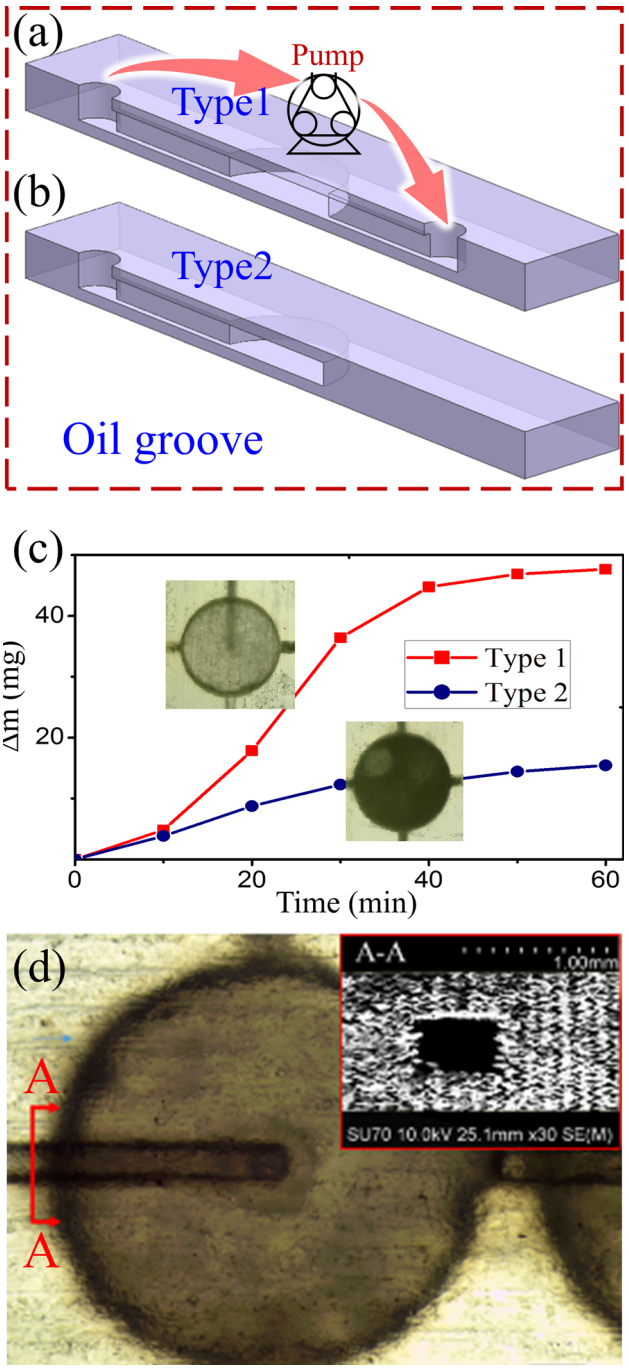

Fig. 4 Schematic of the posttreatment setup to remove the support material. **a** Channel with output port. A circulating pump was connected to each end of the channel. **b** Channel without output port, only immersed in heated oil. **c**. Comparison of removal rates of two structural types when the pump speed is 200 rpm **d** SEM image of the fabricated cross-section

One of the powerful features of this design is its integration. Decoding is the basic application of a digital microfluidic system that converts a series decimal pressure signal into a binary channel switch number. As the number of inputs n increases, the outlets of the decoder increase exponentially from 2 to 2^n. Figure 5a shows a simple 2–4 decoder circuit structure that first designed by Quake et al. which includes 4 triodes and 2 inverters. Four control channels were split into two terms, defined as A (0,1) and B (0,1). The output signal between 0 and 1 that simulated a diode could be switched by connecting the peer term channel to an electromagnetic valve. Each channel (sample or control) contains two valves.

For visualization purposes, four T-type droplet generators were connected to the output of each sample channel. The experimental phenomena were clearly observed as the sample flowed out of each channel with a water-in-oil state. The droplet generator is a "T" junction that separates the sample by applying a shear force (Teh et al. 2008). The printed chip is shown in Fig. 5b.

3 Results and discussion

3.1 Microvalve tests

The experimental testing of the integrated chip to demonstrate the performance of a single flow control unit for the resistance and pressure interactions in different subcircuits is difficult. The valves were produced and measured separately. The membrane deformation was identified via simulation based on finite element analysis. The structural stress was confirmed to be under the elastic limit at a normal deformation of 100 μm. The tensile stress is shown in Fig. 6a, and the ultimate tensile strength of this structural material is 42.4 MPa. Furthermore, we obtained the maximum pressure of 190 kPa by an ultimate tensile strength test (see setup schematic in Fig. 6b, c). All the pneumatic data were measured by a DRUCK PACE 6000 (GE, USA) pressure control and test system.

Next, we characterized the dynamic behavior of the valve by measuring the outlet flow rate through the sample channel. The sample flow was driven by a constant-pressure air supply. The pressure signal was generated by a gas

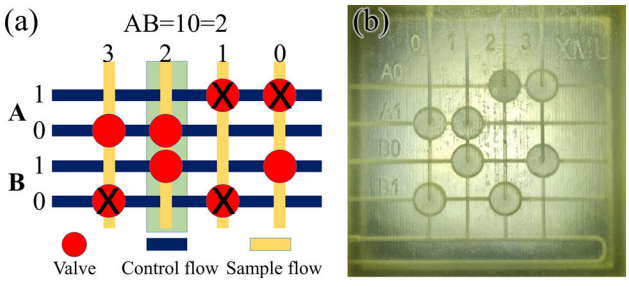

Fig. 5 Schematic of the logic decoding circuit. **a** Logic network principle of a 2–4 decoder in a microfluidic system. Red solid circles in each cross-section represent membrane valves. **b** Photographs of a 3D-printed decoder with no external connections

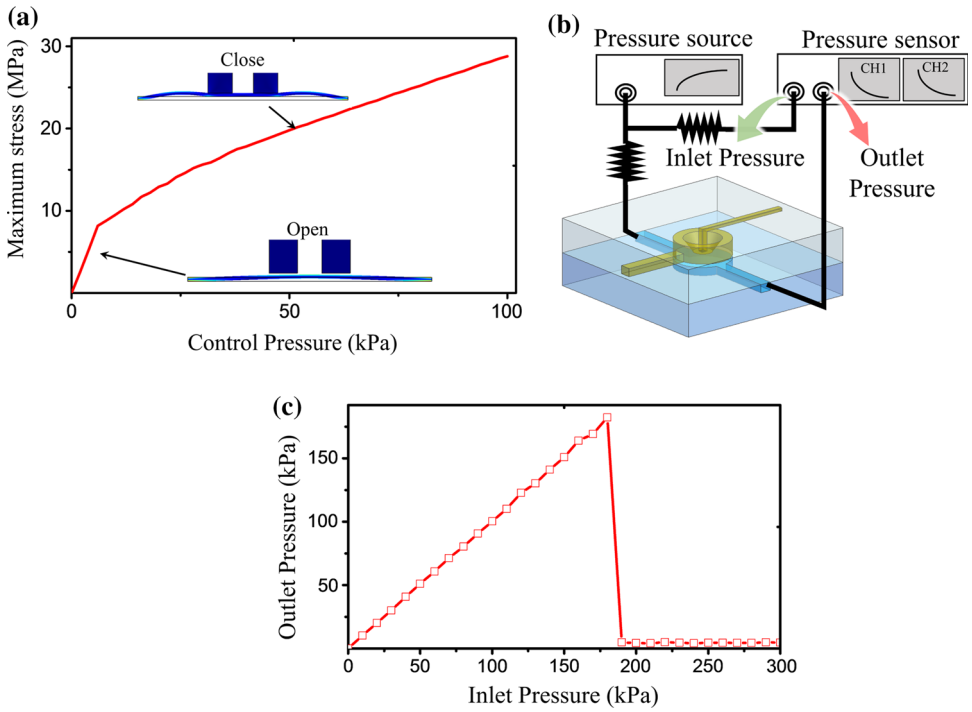

Fig. 6 Membrane reliability test. **a** Membrane stress simulation by COMSOL Multiphysics (COMSOL Inc., Sweden). There is a significant difference in the maximum stress change rate of the membrane during the opening and closing stages of the valve. **b** Devicesetup for ultimate tensile strength experiments. **c** Graph of the pressure through the flow channel when very large pressures are applied to the valve. When the pressure is increased to 190 kPa, the membrane breaks

cylinder and controlled by a proportional solenoid. The sample channel was connected to a syringe pump (Harvard, USA). Several experiments were performed, and the data showed a consistent trend. The closing pressure was approximately 14 kPa for each valve (Fig. 7a). The response frequency, which is a leading indicator for many digital circuits, is also important for microfluidic circuits. We characterized the switch frequency of the valve by measuring the flow rate through the valve for a given oscillator pressure signal. A sharply declining flow rate was measured with decreasing frequency within a certain range at the response point. The distortion point corresponds to the critical frequency. According to the above data, the control pressure was adjusted to 15 kPa, which is slightly higher than the critical close point. The inlet sample flow was fixed at a constant pressure of 1 kPa, and the outlet flow rate was measured under each frequency. The flow rate was 2.8 mL/min when the control pressure was zero. A pulsed square wave was used to drive the valve and regulate its frequency. The duty ratio of the air pressure was 50%. Under ideal conditions, the outlet flow rate was approximately 2.8 mL/min when above the critical frequency and 1.4 mL/min when below the critical frequency. In the experiment, the operating mode of the valve was switched within the range of 2–3 Hz. Accurate measurements indicated that the operating region of the valve is below 2.5 Hz (Fig. 7b).

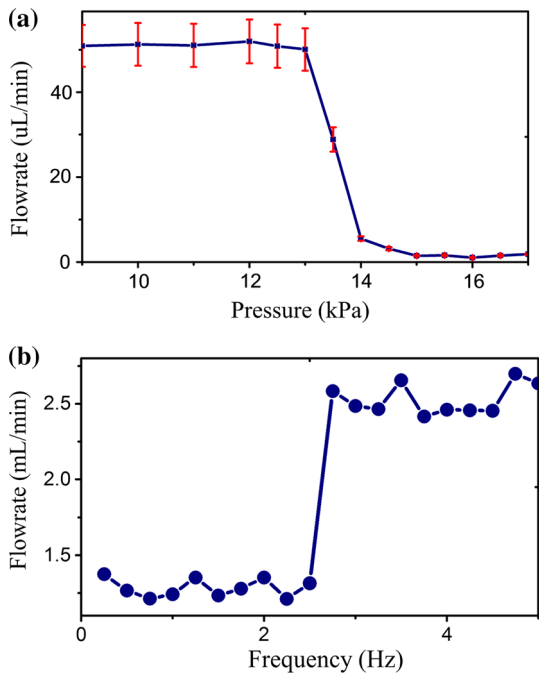

Fig. 7 Flow rate measurements with 600 µm-diam valves. **a** Closing pressure measurement. The membrane was undergoing an operating mode changing process from 13 to 14 kPa and completely closed at a control pressure of 15 kPa. **b** Frequency response curve. The working frequency should be lower than 2.5 Hz to ensure that the outlet flow rate is half of that in the no-pressure condition

3.2 Performance of the microdecoder

Integrated logic gates have widespread use in electrical applications, such as grating rulers, encoders and digital I/Os. The situation is the same in the flow field. A high-frequency or switching performance in flow decoders can be achieved because the material has excellent bio-affinity. A fluidic 2–4 decoder can be built by connecting 8 valves to a common cathode. The membrane is a sensitive element that would unavoidably break during fabrication. These failures are caused by local impact, turbulent flow or fatigue in the wax removal process. A statistical analysis performed on the broken number revealed that the availability ratio of the valve could reach 95%. All of the selected chips were carefully tested in the next experiment. The chip was used to control 4 different inlet samples (replaced by water). All of the valves were driven by a 15 kPa air pump, and the sample flow was connected to a reservoir with a constant pressure of a 1 kPa. Each control group of A (0,1) and B (0,1) was switched by a two-position, four-way solenoid valve. An interference test between each channel was designed to investigate the switching performance. The number of droplets generated from each channel was recorded when the chip operated from code 0–3. The input flow rate was adjusted to 20 μL/min for oil and 15 μL/min for water via an injection pump. Approximately 80 droplets were generated from the working channel per minute, and the same number were accounted for in the outlet. Only a small amount of leakage was observed in the closed channels for each code, particularly in the switching period (Fig. 8a–d). A clearer record is shown in the supplementary information.

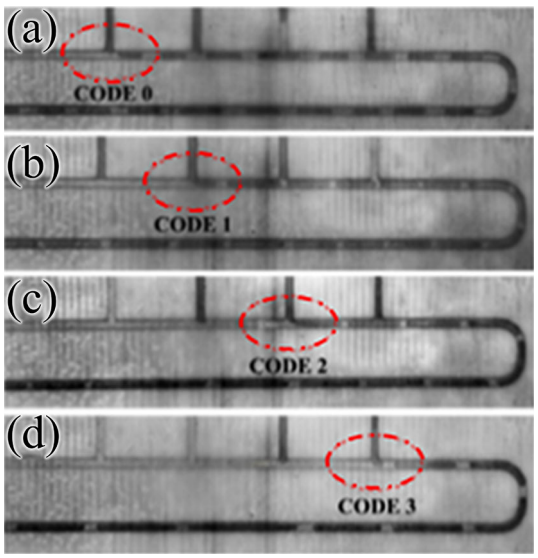

Fig. 8 Microfluidic decoding experimental result for each code

4 Conclusion

In conclusion, we have demonstrated a 3D-printable microvalve structure. This modified version of the original membrane valve is compatible with 3D-printed hard materials. The optimized valve size was calculated by a theoretical equation. The valve was designed with a closing pressure of 14–15 kPa and could continuously operate below a frequency of 2.5 Hz. Compared with the brittle PDMS chip, this 3D-printed device can operate at pressures as high as 190 kPa. The structure and process also have the potential to make large-scale microvalve arrays for logic applications. Similar to an electrical logic circuit, 8 valves in a 6 × 6 mm area with 400 × 600 μm microchannels were integrated to achieve the function of a 2-4 decoder. We were able to decode a fluid 0/1 signal into a channel number signal by controlling the opening and closing of each valve.

Although the printing resolution and scale are still limited by the printers and materials, several valves and an integrated structure could still be printed. Future research could involve the application of a microfluidic pneumatic signal processor as an alternative to electronic circuits. A fluidic processor could be useful in certain fields, such as under a strong electromagnetic field or in an underwater environment, which is necessary for the control of soft pneumatic actuators.

Acknowledgements This work was supported by the National Natural Science Foundation of China (U1505243).

References

Au AK, Bhattacharjee N, Horowitz LF et al (2015) 3D-printed microfluidic automation. Lab Chip 15(8):1934–1941. https://doi.org/10.1039/c5lc00126a

Bhattacharjee N, Urrios A, Kang S et al (2016) The upcoming 3D-printing revolution in microfluidics. Lab Chip. https://doi.org/10.1039/C6LC00163G

Brockmeyer E, Marynel Vázquez, Desai R et al (2015) 3D printing pneumatic device controls with variable activation force capabilities, pp 1295–1304. https://doi.org/10.1145/2702123.2702569

Cheng N (2008) Formulas for friction factor in transitional regimes. J Hydr Eng 134(9):1357–1362. https://doi.org/10.1061/(ASCE)0733-9429(2008)134:9(1357

Cho SK, Fan, SK, Moon H, Kim CJ (2002) Towards digital microfluidic circuits: creating, transporting, cutting and merging liquid droplets by electrowetting-based actuation. In: The fifteenth IEEE international conference on MICRO electro mechanical systems, pp 32–35. https://doi.org/10.1109/MEMSYS.2002.984073

Frank P, Gräfe D, Probst C et al (2017) Autonomous integrated microfluidic circuits for chip-level flow control utilizing chemofluidic transistors. Adv Funct Mater. https://doi.org/10.1002/adfm.201700430

Garcia-Cordero JL, Kurzbuch D, Benito-Lopez F et al (2010) Optically addressable single-use microfluidic valves by laser printer lithography. Lab Chip 10(20):2680. https://doi.org/10.1039/c004980h

Gong H, Woolley AT, Nordin GP (2016) High density 3D printed microfluidic valves, pumps, and multiplexers. Lab Chip 16(13):2450. https://doi.org/10.1039/c6lc00565a

Gong H, Woolley AT, Nordin GP (2018) 3D printed high density, reversible, chip-to-chip microfluidic interconnects. Lab Chip. https://doi.org/10.1039/C7LC01113J

Hua G, Woolley AT, Nordin GP (2016) High density 3D printed microfluidic valves, pumps, and multiplexers. Lab on A Chip 16(13):2450. https://doi.org/10.1039/C6LC00565A

Jain V, Raj TP, Deshmukh R et al (2015) Design, fabrication and characterization of low cost printed circuit board based EWOD device for digital microfluidics applications. Microsyst Technol 21:1–9. https://doi.org/10.1007/s00542-015-2680-7

Jensen EC, Zeng Y, Kim J et al (2010) Microvalve enabled digital microfluidic systems for high performance biochemical and genetic analysis. Jala Charlottesv Va 15(6):455–463. https://doi.org/10.1016/j.jala.2010.08.003

Jia ML, Meng Z, Yeong WY (2016) Characterization and evaluation of 3D printed microfluidic chip for cell processing. Microfluid Nanofluid 20(1):1–15. https://doi.org/10.1007/s10404-015-1688-8

Kadimisetty K, Song J, Doto AM et al (2018) Fully 3D printed integrated reactor array for point-of-care molecular diagnostics. Biosens Bioelectron. https://doi.org/10.1016/j.bios.2018.03.009 **(S0956566318301763)**

Kawai K, Arima K, Morita M et al (2015) Microfluidic valve array control system integrating a fluid demultiplexer circuit. J Micromech Microeng. https://doi.org/10.1088/0960-1317/25/6/065016

Kazenwadel F, Biegert E, Wohlgemuth J et al (2016) A 3D-printed modular reactor set-up including temperature and pH-control for the compartmentalized implementation of enzyme cascades. Eng Life Sci. https://doi.org/10.1002/elsc.201600007

Kim SJ, Lai D, Park JY et al (2012) Microfluidic automation using elastomeric valves and droplets: reducing reliance on external controllers. Small 8(19):2925–2934. https://doi.org/10.1002/smll.201200456

Knowlton S, Yu CH, Ersoy F et al (2016) 3D-printed microfluidic chips with patterned, cell-laden hydrogel constructs. Biofabrication 8(2):025019. https://doi.org/10.1088/1758-5090/8/2/025019

Lederer T, Clara S, Jakoby B et al (2012) Integration of impedance spectroscopy sensors in a digital microfluidic platform. Microsyst Technol 18(7–8):1163–1180. https://doi.org/10.1007/s00542-012-1464-6

Lee JM, Zhang M, Yeong WY (2016) Characterization and evaluation of 3D printed microfluidic chip for cell processing. Microfluid Nanofluid 20(1):5. https://doi.org/10.1007/s10404-015-1688-8

Lee YS, Bhattacharjee N, Folch A (2018) 3D-printed quake-style microvalves and micropumps. Lab Chip. https://doi.org/10.1039/C8LC00001H

Lu YW, Lin PT, Pai CS (2007) Polydimethylsiloxane (PDMS) Bonding Strength Characterization by a Line Force Model in Blister Tests. Solid-State Sens Actuators Microsyst Conf Transducers Int IEEE. https://doi.org/10.1109/SENSOR.2007.4300578

Ma H, Jiang L, et al (2009) A programmable microvalve-based microfluidic array for real-time characterization of neurotoxin-induced responses of individual C. Elegans[C]. Asian-pacific international symposium on microscale separations & Analysis & Asian-pacific international symposium on Lab-on-chip. 2009. https://doi.org/10.1063/1.3274313

Macdonald NP, Zhu F, Hall CJ, Reboud J, Crosier PS, Patton EE, Wlodkowic D, Cooper JM (2016) Assessment of biocompatibility of 3D printed photopolymers using zebrafish embryo toxicity assays. Lab on a Chip 16(2):291–297. https://doi.org/10.1039/C5LC01374G

Moore JL, Mccuiston A, Mittendorf I et al (2011) Behavior of capillary valves in centrifugal microfluidic devices prepared by three-dimensional printing. Microfluid Nanofluid 10(4):877–888. https://doi.org/10.1063/1.3274313

Munshi AS, Chen C, Townsend AD et al (2018) Use of 3D printing and modular microfluidics to integrate cell culture, injections and electrochemical analysis. Anal Methods. https://doi.org/10.1039/C8AY00829A

Oh KW, Lee K, Ahn B et al (2012) Design of pressure-driven microfluidic networks using electric circuit analogy. Lab Chip. https://doi.org/10.1039/C2LC20799K

Rhee M, Burns MA (2009) Microfluidic pneumatic logic circuits and digital pneumatic microprocessors for integrated microfluidic systems. Lab Chip 9(21):3131–3143. https://doi.org/10.1039/b904354c

Rogers CI, Qaderi K, Woolley AT et al (2015) 3D printed microfluidic devices with integrated valves. Biomicrofluidics 9(1):016501. https://doi.org/10.1063/1.4905840

Scott-Murrell E, Lanza D, Schertzer MJ (2017) Dimensionless model for impedimetric sensing of particle laden droplets in digital microfluidic devices. Microsyst Technol 2017:23. https://doi.org/10.1007/s00542-016-3011-3

Sochol RD, Sweet EC et al (2015) 3D printed microfluidic circuitry via multijet-based additive manufacturing. Lab Chip. https://doi.org/10.1039/C5LC01389E

Sweet EC, Chen CL, Karakurt I et al (2017) 3D printed three-flow microfluidic concentration gradient generator for clinical *E. Coli*-antibiotic drug screening. IEEE Int Conf Micro Electro Mech Syst IEEE. https://doi.org/10.1109/MEMSYS.2017.7863376

Teh SY, Lin R, Hung LH et al (2008) Droplet microfluidics. Lab Chip 8(2):198–220. https://doi.org/10.1007/978-0-387-48998-8_371

Thorsen T, Maerkl SJ, Quake SR (2002) Microfluidic large-scale integration. Science 298(5593):580–584. https://doi.org/10.1126/science.1076996

Unger MA, Chou HP, Thorsen T, Scherer A, Quake SR (2000) Monolithic microfabricated valves and pumps by multilayer soft lithography. Science 288(5463):113–116. https://doi.org/10.1126/science.288.5463.113

Wehner M, Truby RL, Fitzgerald DJ et al (2016) An integrated design and fabrication strategy for entirely soft, autonomous robots. Nature 536(7617):451–455. https://doi.org/10.1038/nature19100

Zhu F, Macdonald NP, Cooper JM, Wlodkowic D (2014) Additive manufacturing of lab-on-a-chip devices: promises and challenges. In: Friend J, Hoe Tan H (eds) Proceedings of SPIE, Micro/Nano materials, devices, and systems, vol 8923. SPIE-International Society for Optical Engineering, Melbourne, Australia, pp 1–14. https://doi.org/10.1117/12.2033400

Zhu F, Skommer J, Macdonald NP et al (2015) Three-dimensional printed millifluidic devices for zebrafish embryo tests. Biomicrofluidics 9(4):368–373. https://doi.org/10.1063/1.4927379